Traffic & Transportation

Aerodynamics of Freight Trains – Addressing the Complexity of Train Geometry through an Open Database

Luca CORNIANI[1], Paolo SCHITO[2], James BELL[3], Joao POMBO[4], Stefano BRUNI[5]

Original Scientific Paper
Submitted: 9 Sep 2025
Accepted: 4 Nov 2025
Published: 29 Jan 2026

[1] Corresponding author, luca.corniani@polimi.it, Department of Mechanical Engineering, Politecnico di Milano, Milan, Italy
[2] paolo.schito@polimi.it, Department of Mechanical Engineering, Politecnico di Milano, Milan, Italy
[3] james.bell@dlr.de, German Aerospace Centre (DLR), Institute of Aerodynamics and Flow Technology, Göttingen, Germany
[4] j.pombo@hud.ac.uk, Department of Engineering, University of Huddersfield (HUD), Huddersfield, United Kingdom
[5] stefano.bruni@polimi.it, Department of Mechanical Engineering, Politecnico di Milano, Milan, Italy

Publisher:
Faculty of Transport and Traffic Sciences, University of Zagreb

ABSTRACT
The study of the aerodynamics of freight trains is important for safety, efficiency and reducing damage during the operation of freight trains. It is also very important for the accurate estimation of drag resistance and, correspondingly, of the required traction effort. Computational fluid dynamics (CFD) is often used to investigate air flows around a freight train and their effects on vehicle dynamics, especially on drag, slipstream and pressure pulses in tunnels. Most of these studies, however, considered container wagons, while a much wider variety of wagon types are currently used. Therefore, there is a need for further research investigating the aerodynamics of more freight train geometries. This involves intensive work investigating realistic wagon geometries and generating representative generic versions. Subsequently, a complex freight train can be generated from these generic building blocks. To address the need for efficient production of these consists, a database of representative wagon and locomotive geometries was created. In this work, the geometry database is presented and is used to generate realistic freight train geometries suitable for CFD analyses. Then, selected results of CFD simulations performed using the geometries generated from the database are presented, demonstrating the use of the tool.

KEYWORDS
train aerodynamics; CFD; freight trains; container; geometry database.

1. INTRODUCTION

In its white paper [1] the European Union outlines its goals for shifting the transport of freight from road to rail or waterways (both responsible for less CO_2 emissions for each tonne-kilometre (tkm) than trucks [2]). The pursuit of this goal entails the eventual increase in the speed of freight trains to at least 160 km/h (Geischberger et al. [3]).

However, faster freight trains mean that aerodynamic effects, traditionally believed to be almost negligible, become important and raise new design and operation challenges. Research from Quazi et al. [4] and Alam et al. [5] shows that freight trains encounter wind from yaw angles mostly below 20°, and therefore, the main component of the aerodynamic force on a moving train is drag. This means that, with the increase of service speed, aerodynamic resistance becomes the major factor affecting the cost and environmental impact of train operation, considering that already at current service speeds aerodynamic resistance forces account for most of the overall resistance to forward motion [6] and that aerodynamic resistance grows with the square of the speed. Moreover, with the increase of service speed, other aerodynamic issues become noteworthy, namely

the effect of crosswinds leading to the risk of derailment or overturning and slipstream effects, i.e. the effects caused by the air dragged along by the freight train while it runs on the railway track [7, 8].

Unlike streamlined passenger trains, freight trains behave as bluff-bodies, and thus the flow around these vehicles is more turbulent and intrinsically unsteady. The study of freight train aerodynamics is further complicated by the fact that they can be composed of a variety of wagons with diverse geometries and that local differences in wagon or train geometry may have deep impacts on the above-mentioned aerodynamic effects. For instance, drag is highly sensitive to the shape of the wagons and particularly to the presence of large gaps between containers in intermodal container trains, see Maleki et al. [9]. Similarly, slipstream velocities generated by intermodal container trains tend to increase for larger gaps (Flynn et al. [10], Bell et al. [11] and Li et al. [6]) and, in the presence of crosswinds, these effects may be severe to the point of destabilising people standing in the wake of the train (Flynn et al. [7]).

The aerodynamics of freight train has been studied in the literature with both numerical and experimental methods.

Most experimental studies on freight trains are conducted in wind tunnels. Alam et al. [12–14] performed a wind tunnel test on a 1:15 scale model of a double-stacked container wagon in isolation, while Siegel et al. [14], Buhr et al. [13] and others used wind-tunnel experiments to study freight trains in different consists. Subsequent studies by Giappino et al. [8, 15], Kocon et al. [16] and Alam et al. [5] focused on the risk of overturning caused by crosswind on freight trains at different yaw angles and gap sizes. Wind tunnel tests have also been used by Soper et al. [17] and Sterling et al. [8] to study the slipstream velocities generated by freight trains and found them to be much greater than what was observed in passenger trains. Soper et al. [18] used full-scale experiments to compare the aerodynamics of passenger and freight trains and found that freight trains at modest speed generate slipstream velocities higher than the passenger trains (although not in violation of the TSI regulations).

CFD methods have been developed throughout the years to compute numerical solutions of the governing equations of fluid flow around a solid body and the aerodynamic forces acting on the body. For industrial applications, the equations are often averaged over time and are called Reynolds-averaged Navier-Stokes (RANS) equations. Steady and unsteady RANS solvers exist (noted as URANS in the unsteady case) that solve these equations using the finite volume method. An alternative formulation called large eddy simulations (LES) resolves only the largest structures of the flow, while taking advantage of some universal properties of turbulent flows for capturing the effect of small-scale phenomena. The LES method is less straightforward and more computationally demanding than URANS, but it is more accurate, especially in resolving strongly turbulent flows. This method is therefore more often used in research applications. Finally, hybrid methods have been devised that resolve the flow using the URANS and LES formulations in different parts of the domain, to obtain the best trade-off between accuracy and computational cost. Some examples of these methods are embedded large eddy simulation (ELES), detached eddy simulation (DES) and delayed detached eddy simulation (DDES). *Table 1* summarises the properties of the main CFD methods, see reference [19] for more details.

Table 1 – Overview of CFD methods and their properties

Method	Numerical approach	Advantages and disadvantages
RANS	The governing equations are approximated with algebraic equations and solved. Time-dependent terms are neglected.	— Modest computational cost — Unsuitable for strongly unsteady flows — Modest accuracy
URANS	A time average operator is applied on Reynolds-averaged governing equations, removing the time dependency only on the time scales typical of turbulent fluctuations. Unsteady behaviour typical of larger time scales is still captured.	— Medium computational cost — Most suitable for the computation of aerodynamic forces — Modest accuracy for turbulence flow properties
LES	Flow is described as the sum of 'eddies' and the equations are formulated in the inverse-of-eddy-dimension domain (via Fourier transforms). Kolmogorov hypotheses for small-scale turbulence are used to model small-scale behaviour.	— High accuracy in both aerodynamic forces and flow properties — High computational cost (typically excessive for industry applications) — Hybrid methods available

Different works have been published that compared the accuracy and cost of different methods (Wang et al. [20], and Maleki et al. [21]), and they showed that RANS is unsuitable for the simulation of freight trains

because of the pronounced unsteadiness of the flow. More computationally intensive methods, such as LES, ELES, DES or DDES, are generally agreed to be most accurate, predicting flow topology and aerodynamic coefficients in line with experimental results, whilst URANS has shown an intermediate level of accuracy and computational cost between RANS and LES. It should be noted, however, that while RANS methods fail to predict the numerical value of aerodynamic coefficients, they predict their trends and are suitable for comparing the performance of different geometries (Maleki et al. [21]).

The Academics4Rail research project, funded by the European community under the Europe's Rail funding programme, has launched a comprehensive investigation into freight trains' aerodynamics. The objective is to define guidelines for the creation of CFD models of freight trains, analyse different realistic operation scenarios and synthesise the results in guidelines for safer and more efficient operation of freight trains with regard to aerodynamic effects.

Given the breadth of the problems addressed, the need for the efficient definition of geometric models for single vehicles (locomotives and wagons) and for complete freight trains becomes apparent. Therefore, the first part of the research was devoted to creating an open database of geometries for vehicles and vehicle parts in formats that are compatible with software for CFD simulation. In this way, complex geometries of freight train consists that are representative of realistic freight operation scenarios can be efficiently created. In the creation of the database, vehicle geometries are designed with different levels of detail, allowing the efficient creation of simpler and more detailed CFD models, in view of finding a trade-off between accuracy and computational efficiency. The database is made available in open form to all interested users, following the example of previous projects in other industries such as automotive (the DrivAER project, by Heft et al. [22]), cycling (Terra et al. [23]) and aerospace (Giannellis et al. [24] and Bykerk [25]).

This paper presents the current (September 2025) version of the geometry database and demonstrates its use in the context of CFD analyses, considering geometries representative of a typical intermodal container. In further updates, more levels of detail will be added for some geometries and pressure distributions will be made available for specific consists. The paper is structured as follows: in Section 2 of the paper, a detailed description of the geometries and the process by which they have been created and stored in the database is provided. In Section 2, the methodology for the construction of the database and for the CFD simulations is outlined, while in Section 3, the results of the simulations are presented and discussed. Finally, in Section 4 conclusion and final remarks are drawn.

2. METHODOLOGY

Unlike passenger trains, freight trains exhibit a wide variety of geometries resulting from mixes of different wagon types having very diverse features and shapes. Therefore, the investigation of air flows around these vehicles needs to be supported by suitable tools addressing the efficient generation of the 3D geometry required as input. In this section, the creation and features of the geometry database will be outlined.

2.1 The database of freight train geometries

For CFD simulations, the complexity of the model has an impact on the computational cost; therefore, a careful trade-off between fidelity to the real geometry and computational cost needs to be considered.

Some level of defeaturing, i.e. a simplification of the geometry used in the CFD model, needs to be implemented to keep the complexity and size of the CFD model within limits that allow its numerical solution with the computer resources available. Determining the proper level of defeaturing involves an iterative process in which the same nominal geometry is modelled at different levels of detail. Therefore, the process used to create the 3D geometry for the CFD model shall be able to consider wagon shapes at different levels of detail.

To address the above-described needs and taking inspiration from the approach followed by other industries, an open database of freight train geometries was created. The database has been devised as a modular and expandable repository of 3D geometries that can be combined to form the geometric model of a single wagon or of a complete freight train seen as the composition of one or more locomotives and a generic number of wagons. The approach followed is to consider each vehicle, either a locomotive or a wagon, as formed by different components or modules that can be mixed to generate a wide variety of geometries. For each module and for each vehicle type, different levels of detail of the model are available, facilitating the generation of the CFD model for the same freight vehicle/train for different defeaturing levels. The modular

approach followed in the definition of the geometry database offers several advantages: it facilitates the efficient and fast production of many diverse freight train geometries while allowing the user to easily apply the desired level of defeaturing and enables the efficient and interactive comparison of alternative modelling options.

To define the database structure, a categorisation of freight wagons is introduced. While no official classification exists, based on the examination of freight wagons presently in service in European countries [26], the following categories are considered:

1) Open wagons;
2) Covered wagons;
3) Flat wagons;
4) Dump cars;
5) Tank wagons;
6) High-capacity wagons.

Locomotive geometries instead are proposed in the database in three different versions (types A, B and C), their geometry being defined based on locomotives widely used for hauling freight trains in Europe. *Figure 1* shows the three locomotive variants at the highest level of detail.

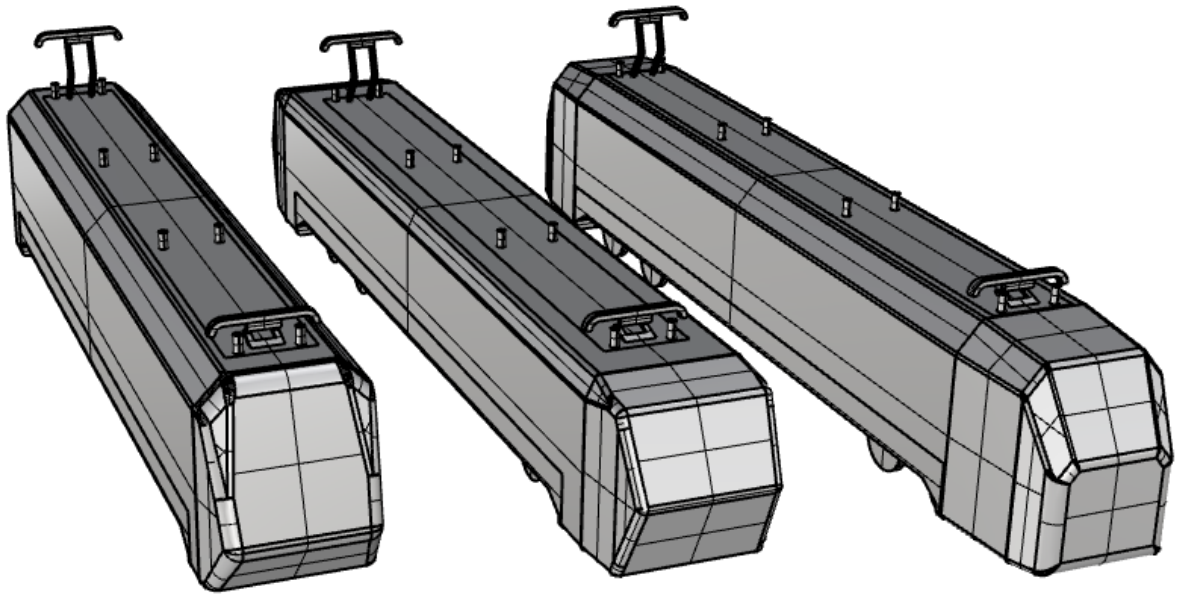

Figure 1 – From left to right, types A, B and C locomotives in the highest level of detail.

Two examples of convoys assembled with the geometries of the database (composed of locomotive type C, followed by different types of wagons) are presented in *Figure 2*.

All wagons are defined as being composed of three parts, from bottom to top, the running gear (i.e. the wheelsets, bogies and suspensions), the deck (consisting of a platform resting over the bogies) and the cargo (i.e. the structure/container or tank over the deck). For flat wagons, only the running gear and deck are included. In *Figure 3,* the components of the wagon are shown for the dump car wagon (on the left) and the components of the B version of the locomotive (on the right) are shown.

Locomotives are characterised by more similar geometric features but still show significantly different shapes in their frontal region, which is very relevant to the flow structure and aerodynamic forces. Also, for the locomotives, the entire geometry is split into three parts, i.e. from bottom to top, the underbody (including the running gear), the main body and the roof (including the pantograph). The pantograph has been modelled according to the dimensions reported by Baker et al. [27]. Finally, *Figure 4* and *Figure 5* show the alternative defeaturing options available for modelling, respectively, the running gear of a wagon (limited to one single Y25 bogie) and the underbody and roof of the locomotive with reference to locomotive type A.

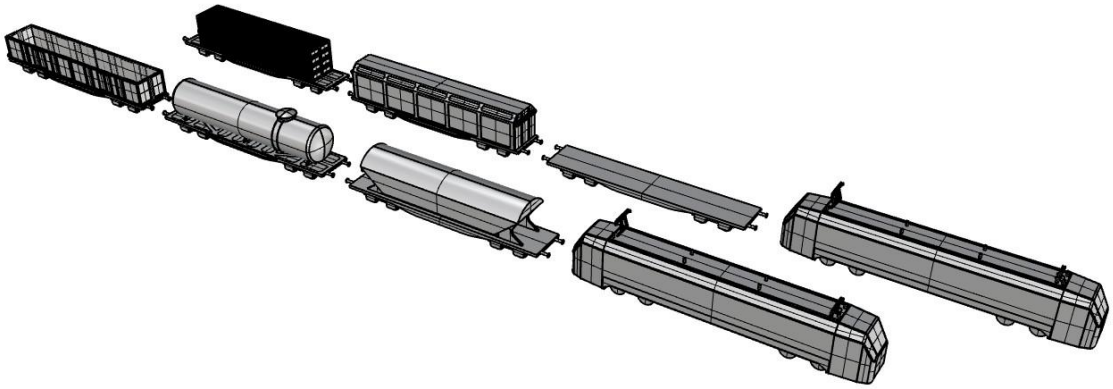

Figure 2 – Two train consists of different types of wagons with the highest level of detail. At the head of both is the C version of the locomotive with the highest level of detail.

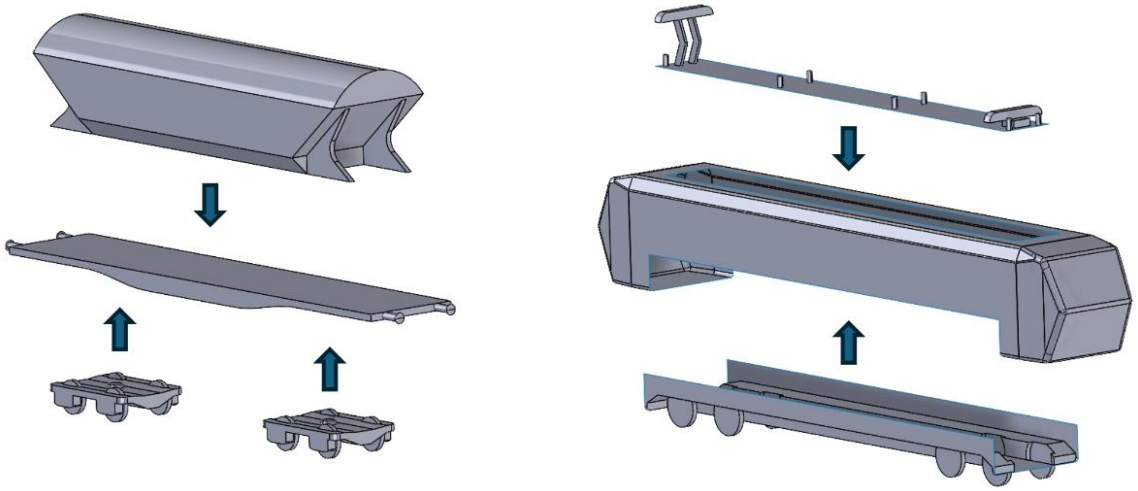

Figure 3 – Components assembly of wagons (left) and locomotives (right)

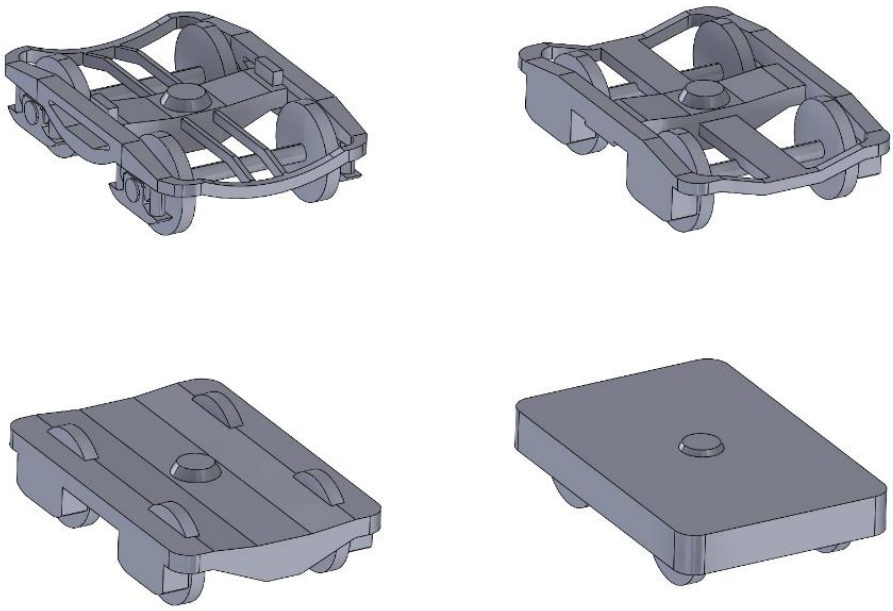

Figure 4 – Bogies models in different levels of detail

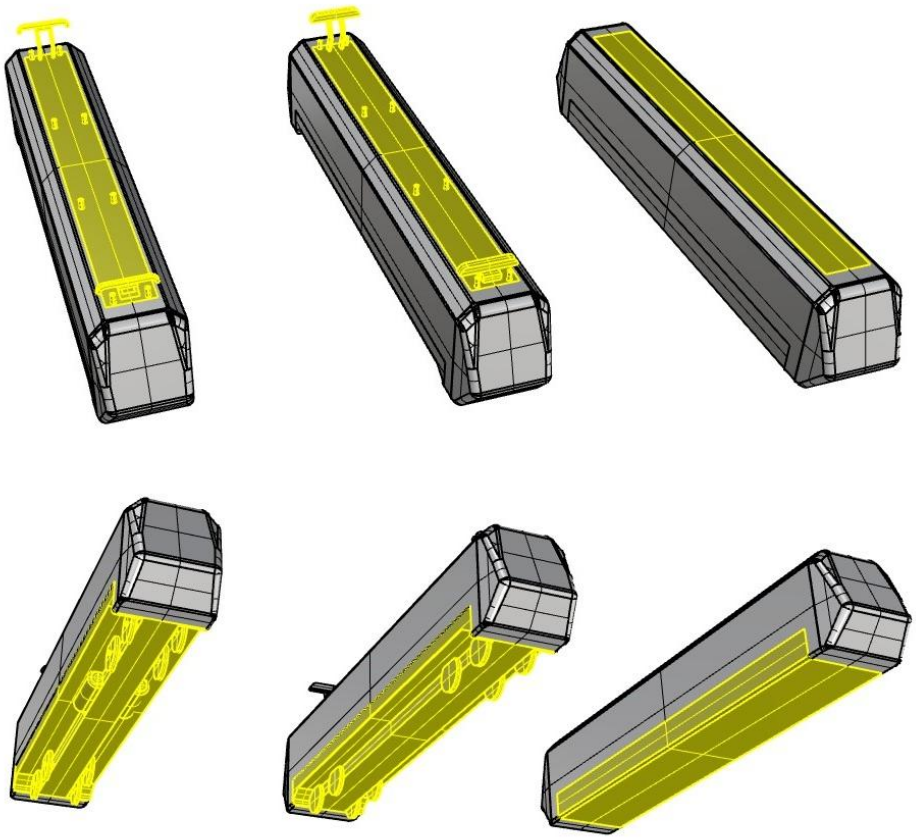

Figure 5 – Roof components and underbody components (both respectively in yellow) in decreasing level of detail from left to right

All the geometries showcased in this work have been made available in STEP format in a public GitHub repository (see Corniani et al. [28, 29], https://github.com/lCornianiPolimi/A4R-Freight-Train-Model-Geometries). A preassembled full wagon with consistent levels of detail among the components has been prepared and uploaded, as well as the single components in all levels of detail. Further additions are still possible (e.g. double-stacked containers, longer versions of covered and flat wagons).

CFD use cases

In this section, some use cases of some of the database geometries will be provided. First, the simple case of a stationary single container wagon with a 40 ft container wagon in a 160 km/h airflow is considered; second, a train of one locomotive and three wagons will be considered. In the latter case, the first wagon behind the locomotive will be composed of a less-detailed flat wagon and container, to compare the results with the single wagon.

The simulations on the single wagons have been carried out using the open-source software OpenFoam v10. In order to reduce computational time, a first steady simulation was run to allow the development of a wake as a suitable initial condition for the numerical simulation of the unsteady flow. This flow solution was not realistic, given the transient nature of the actual flow, but it was more similar to a realistic flow than the potential flow solution (which instead was the starting condition for the steady simulation). The steady state simulation was carried out with the SIMPLE algorithm (see reference [19]) solving the Navier-Stokes equations with the k-ω shear stress transport (SST) turbulence model.

Starting from the solution of the steady solver, the unsteady simulation was run with the same model adopted for the steady-state run. The unsteady simulations were carried out with the PIMPLE algorithm (see reference [19]), with the implicit Euler scheme used for the time derivative.

Figure 6 shows the domain dimensions in terms of lengths (L), widths (W) and heights (H) of the wagon. For the ground and the wagon patches, a wall condition is defined, with a zero-gradient boundary condition for pressure and a no-slip condition (meaning stationary ground) for velocity and turbulence variables. The inlet velocity is set to 160 kmh^{-1}, and at the outlet, a null gauge pressure is imposed. Zero-gradient for pressure and slip condition for velocity were set on all remaining patches.

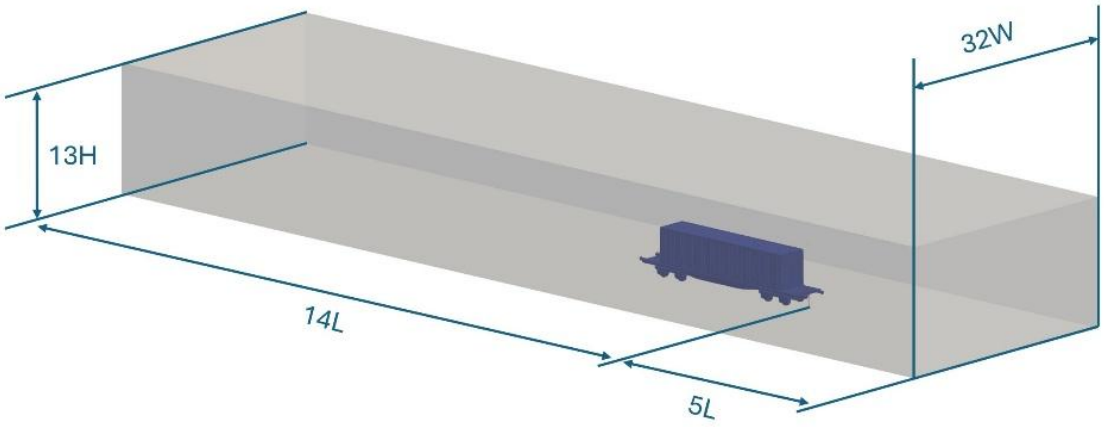

Figure 6 – Simulation domain (not to scale)

The mesh is built using the snappyHexMesh utility, using a top-bottom strategy, with the cells trimmed by the wagon geometry. The structured background mesh is refined in relevant regions around the wagon, in particular around edges and in the wake.

2.2 Mesh independence study

A convergence study is carried out with steady solvers on the single wagons (the same settings and refinement level will be deemed adequate for the multiple-wagon simulations). Mesh independence has been assessed by progressively decreasing the size of all cells while maintaining the size of the domain and the refinement regions constant. *Table 2* reports the lift and drag aerodynamic coefficients determined from steady-state simulations with progressively finer meshes, resulting in a larger number of cells. The coefficients have been calculated using a reference area of 10 m^2 according to *Equation (1)*:

$$C_D = \frac{2D}{\rho A {U_f}^2} \qquad C_L = \frac{2L}{\rho A {U_f}^2} \qquad C_S = \frac{2S}{\rho A {U_f}^2} \tag{1}$$

where D, L and S are the drag, lift and side force on the entire wagon, respectively, ρ is the air density, A is the reference area and U_f is the freestream velocity (44.44 ms^{-1}).

Table 2 shows the force coefficients for drag and lift on the single wagon: the coefficients show remarkable convergence despite the stationary solver. The variations of aerodynamic coefficients remain below 1% beyond the 11.9 million cells grid, thus the results are deemed to be mesh independent beyond this level of refinement. It will be assumed that this level of refinement is suitable for the unsteady solver as well.

The convergence of the force coefficients to a given value is not sufficient to infer the accuracy of that value; indeed, because the flow around freight wagons is strongly unsteady, it should be expected that the steady-state solver will not be able to accurately predict the value of the aerodynamic forces. This is a well-known limitation of the RANS method that has been demonstrated before by Maleki et al. [21].

Table 2 – Convergence of aerodynamic coefficients computed using progressively finer meshes of the volume

Number of cells [millions]	C_D [-]	C_L [-]	$\Delta C_D/C_D$ [%]	$\Delta C_L/C_L$ [%]
2.9	0.809	0.207	+0.24%	-6.94%
4.4	0.811	0.192	+0.44%	+5.84%
6.3	0.814	0.204	+0.65%	+8.04%
8.9	0.819	0.220	-0.06%	+1.08%
11.9	0.819	0.222	-0.53%	-0.63%
15.6	0.815	0.221	+0.59%	-0.44%
20.1	0.819	0.220		

The URANS method is capable of capturing the unsteady nature of the flow and, therefore, is more suitable for the simulations of flows around bluff bodies such as container wagons. The greater accuracy of the URANS method with respect to steady RANS has been shown in the literature before (although they share similar limitations in the prediction of the flow topology, see Wang et al. [20] and Maleki et al. [21]).

After having defined a CFD workflow, the same methodology was applied to analyse a multiple-wagon use case. A train composition of three vehicles was studied: a locomotive followed by three wagons, as shown in *Figure 7*.

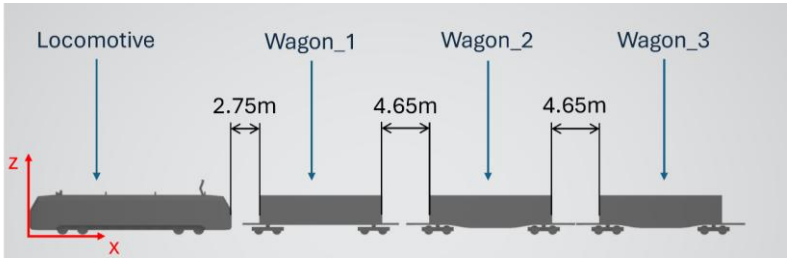

Figure 7 – Train composition of multi-vehicle simulation

In this simulation, the effects on the force coefficients of vehicles joint in this composition will be investigated, with special attention on the trailing wagons.

The first wagon (indicated in *Figure 7* as wagon_1) is designed with the less detailed components, while the trailing wagons (indicated in *Figure 7* as wagon_2 and wagon_3) are made with medium-detailed components. This decision is motivated by the fact that the vehicles of interest for this use case are wagon_2 and wagon_3, while wagon_1 and the locomotive are useful only for producing a sufficiently realistic wake. This is an example of how different levels of detail in the geometries allow the user to customise the setup in order to balance the computational cost and accuracy of the simulation. The C version locomotive is used, while the wagons are flat wagons with containers as cargo.

The gaps between the vehicles have been reported in *Figure 7*, with the gap between the locomotive and wagon_1 being equal to approximately 1.1 wagon widths and the gap between successive containers being equal to approximately 2 wagon widths.

The mesh is constructed with the same level of refinement as the single wagon, and the solver settings are unchanged.

3. RESULTS AND DISCUSSION

In this section, the results from the simulations on the single wagon and the convoy are reported. Furthermore, some discussion of the results will be provided.

3.1 Single wagon

In *Table 3*, the results of URANS runs on a single wagon with two levels of detail are shown. These results show a significant improvement in accuracy with respect to the RANS method, and in fact are comparable to results in the literature obtained with much more accurate methods (see, for example, Östh et al. [30] who obtained a drag coefficient value of 0.90).

Finally, *Figure 8a* shows the magnitude of the mean velocity field in the xz-plane. *Figure 8b* and *Figure 8c* show the x component of the mean velocity profiles on top of the container for the less detailed wagon and the medium detailed wagon, respectively. White lines have been provided in *Figure 8a* to showcase where the mean velocity has been sampled, as well as a more convenient coordinate system for the graphs. From this figure, it is easy to see that the length of the recirculation bubble predicted in both cases is similar, but longer for the medium-detailed case.

Table 3 – Time-averaged aerodynamic coefficients from unsteady, single-vehicle simulations

	C_D [-]	C_L [-]	C_S [-]
Less detailed wagon	0.925	-0.039	-0.004
Medium detailed wagon	0.995	0.028	0.002
Locomotive	0.306	-0.062	-0.002

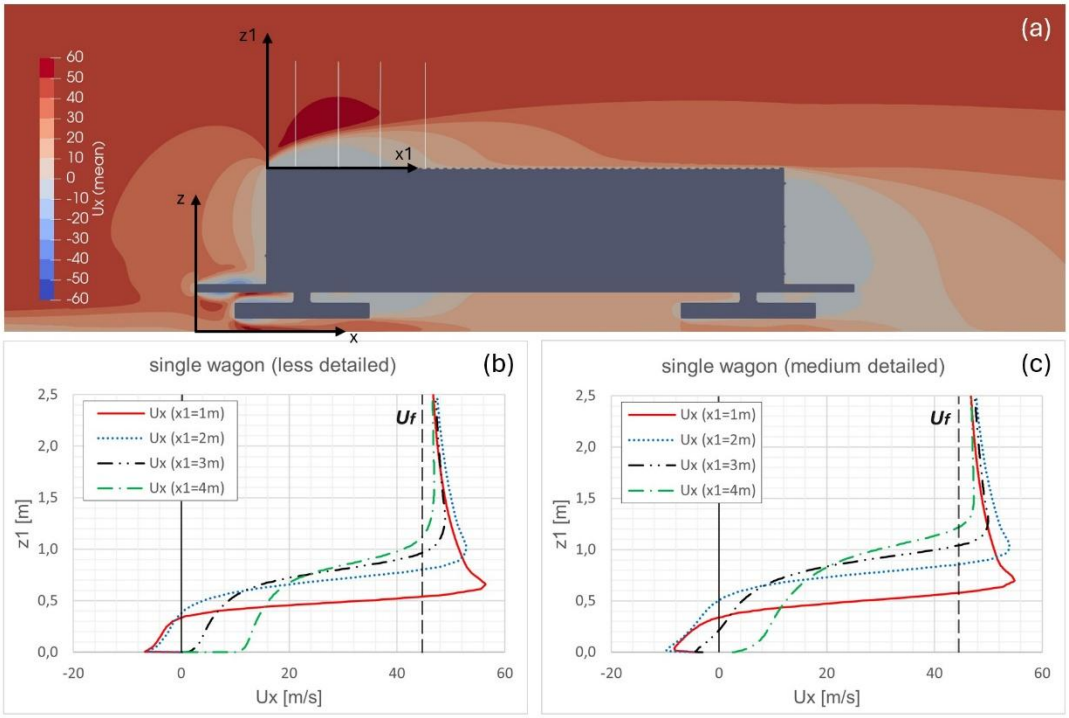

Figure 8 – x component of mean velocity field: a) x component of the mean velocity field around the medium detailed wagon (unsteady simulation); b) velocity profile within recirculation bubble at 1 m, 2 m, 3 m and 4 m from the edge of the less detailed container; c) velocity profile within recirculation bubble at 1 m, 2 m, 3 m and 4 m from the edge of the medium detailed container

3.2 Multiple wagons

The aerodynamic force coefficients on all the vehicles involved are reported in *Table 4*, while the mean pressure coefficient in the flow and the cumulative drag coefficient along the direction of the flow are shown in *Figure 9*. In the cumulative drag plot, three vertical bands have been added to show the position of the containers (in the case of the locomotive, of the full vehicle).

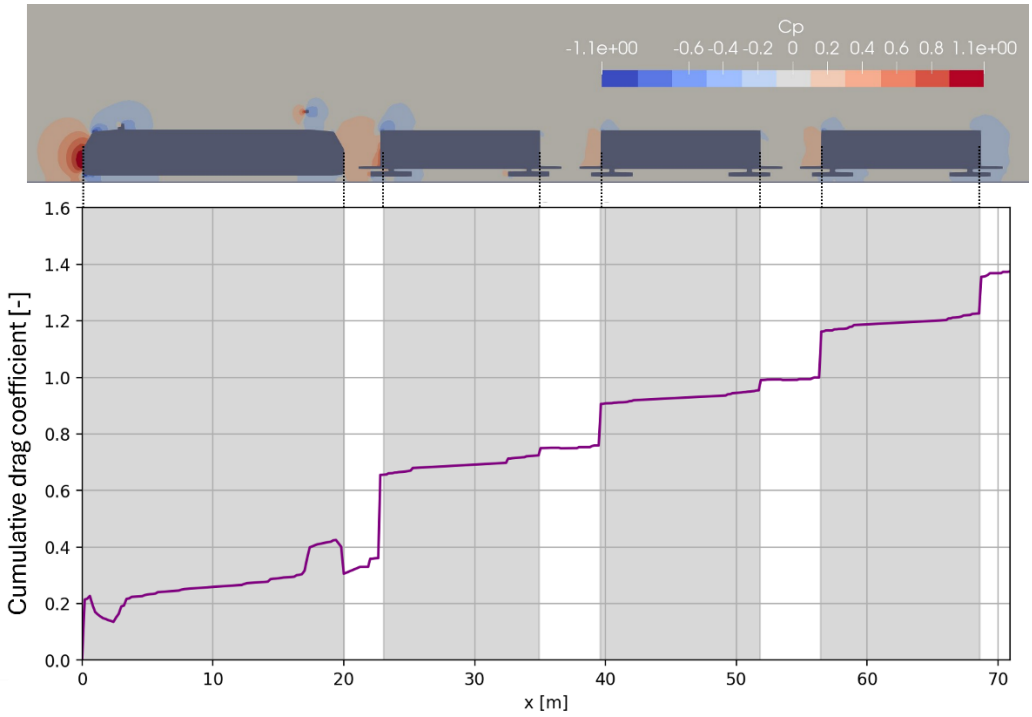

Figure 9 – Comparison of pressure coefficient within the flow and cumulative drag coefficient along the convoy in the direction of the flow

Table 4 – Aerodynamic force coefficients on vehicles of multi-vehicle simulations

Vehicle	C_D [-]	C_L [-]	C_S [-]
Locomotive	0.306	-0.040	-0.007
Wagon_1	0.443	0.077	0.002
Wagon_2	0.242	-0.012	0.005
Wagon_3	0.383	-0.053	0.004

As can be observed in *Table 4*, for all wagons the drag coefficients are lower than the ones obtained in the single-vehicle simulation. This is expected due to the wake of the upstream vehicles. As the flow proceeds along the convoy, the boundary layer progressively develops, transferring its momentum to the vehicles. As a consequence, the drag coefficient of wagon_2 is even lower than wagon_1 because it faces a slower flow. The drag coefficient of wagon_3 increases with respect to wagon_2. The greater drag of the last wagon, however, is mostly explained by the fact that the flow region downstream of it has lower pressure than the gaps between containers, and not because of the flow impacting the front face of the container on wagon_3. This can be seen by observing *Figure 9*, in which the low-pressure region is visible behind the last wagon. In the same figure, the cumulative drag coefficient of the train along the direction of the flow is shown, and the contribution to the drag corresponding to the front and back faces of the container on wagon_3 can be seen. The increase in drag relative to the front face of the last container is very similar to the corresponding increase with wagon_2, while the increase in drag corresponding to the back surface of wagon_3 is much greater than for the other two.

It should be noted when comparing force coefficients of the different wagons, that wagon_1 is subject to a different flow than the other because it is downstream of a different geometry. This difference is showcased in the different pressure distribution on the surface containers, as shown in *Figure 10*, where the time-averaged pressure coefficient on the surface (as defined in *Equation 2*) is shown.

$$C_p = \frac{p - p_f}{\frac{1}{2}\rho {U_f}^2} \tag{2}$$

where p is the time-averaged static pressure of the flow, p_f is the time-averaged static pressure of the freestream flow (in the simulation, this quantity was set to zero).

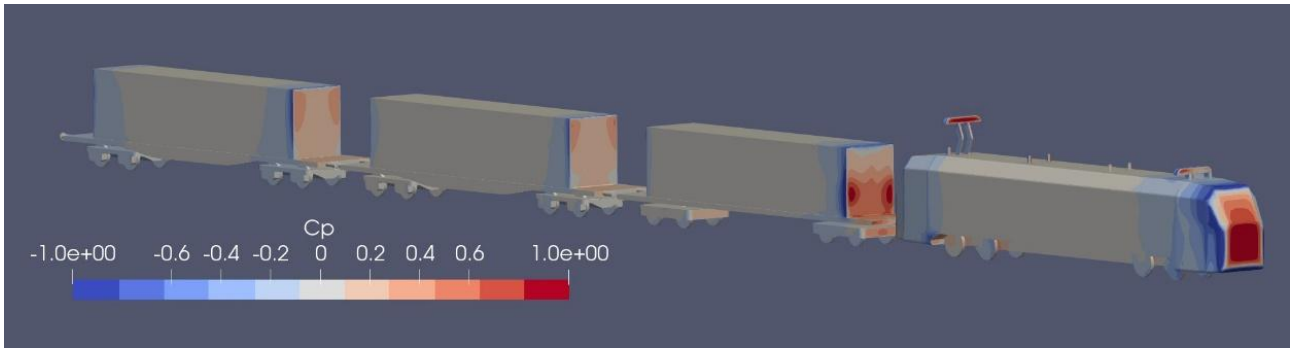

Figure 10 – Time-averaged pressure coefficient on the geometry surface in unsteady multi-vehicle simulation

The Cp distributions shown in *Figure 9* and *Figure 10* are consistent with the decrease in drag coefficient of the wagons. High-pressure regions are present upstream of all vehicles; however, the effect is less pronounced as the vehicle is more distant from the train nose. Due to the interaction between upwind and downwind vehicles, the middle wagons have a mutual interaction, while the last wagon is followed by a low-pressure region that increases the drag. The front pressure coefficient of the first container has a very different distribution from the other two. This fact is caused by the different geometry of the locomotive and makes comparisons between the containers more difficult. However, it can be observed that regions of higher pressure (reaching approximately a Cp of 0.85) are present in the front face of the first container. The second and third containers, instead, have a very similar pressure distribution, and the magnitude of the Cp on their front surfaces is very similar (with maximum values of less than 0.45). As stated before, the greater drag of the last wagon is caused by the low pressure on the back face of the last container.

In *Figure 10*, regions of low pressure are visible immediately downstream of the corners of the front face of each container. These regions confirm the presence of recirculation bubbles that take place where the air flows away from the stagnation region in the front, causing flow separation at the corners.

Bluff bodies, such as container wagons, experience high drag because they create highly separated flow regions, and the gap between containers tends to carry more air with them as they pass through it. This follows from the conservation of momentum, since the aerodynamic drag experienced by the wagon is equivalent to the rate of momentum transferred by the wagon to the surrounding air.

In *Figure 11*, the time-averaged total pressure coefficient (C_{pt}) field is shown. This quantity is defined in *Equation 3*, and it quantifies the variation in the total pressure of the flow with respect to the freestream.

$$C_{pt} = \frac{p_{tot}}{p_{tot,f}} = \frac{p + \frac{1}{2}\rho U^2}{p_f + \frac{1}{2}\rho {U_f}^2} \tag{3}$$

where p_{tot} is the time-averaged total pressure, $p_{tot,f}$ is the time-averaged freestream total pressure, and U is the time-averaged magnitude of the speed of the flow.

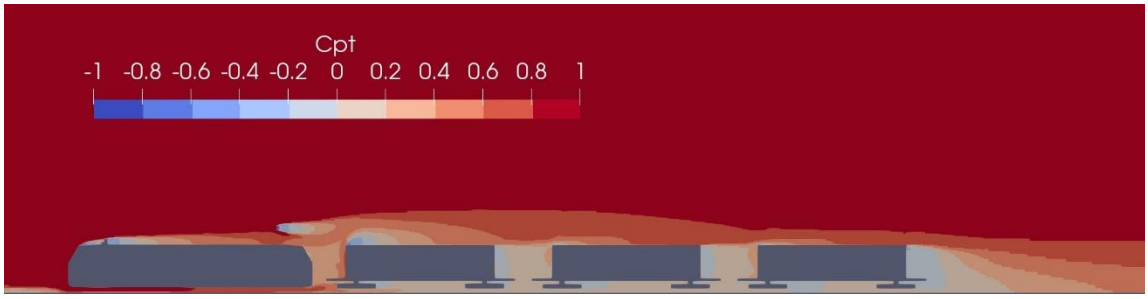

Figure 11 – Time-averaged total pressure coefficient field in unsteady multi-vehicle simulation

By observing *Figure 11*, it is possible to identify the regions of the flow where there are losses of total pressure and thus identify regions of high turbulence. All three vehicles display a flow separation at the upstream top edge; however, the separation is visibly smaller in the downstream wagons than in wagon_1. This is again explained by the reduced velocity in the flow.

4. CONCLUSIONS AND CONTRIBUTIONS

In this work, a database of realistic freight wagon and locomotive geometries has been proposed, with the purpose of offering a quick and efficient way of producing geometries for CFD. The proposed geometries are representative of different realistic vehicles, but can also be assembled with custom levels of detail in different parts. Different types of wagons and locomotives are made available in the database, allowing for the simulation of trains that are realistic in composition too (instead of being only composed of container wagons).

In this work, some CFD simulations were also conducted as a demonstration of the use of the database. The flow around single wagons has been simulated (with steady and unsteady solvers) and has been compared to the flow around the same geometries in a train. In the multiple-vehicle simulation, a lower level of detail has been chosen for the upstream wagon than the downstream ones, further demonstrating the versatility of the database for the construction of geometries that balance accuracy and computational cost.

Finally, the flow around the vehicles has been shown and discussed, particularly the flow around multiple vehicles. Some of the major structures expected in the flow (e.g. the recirculation regions at the corners of the vehicles or the stagnation regions in front of them) have been identified, and the drag coefficients have been found to decrease as the vehicle was placed further from the nose of the train.

ACKNOWLEDGEMENTS

Funded by the European Union. Views and opinions expressed are, however, those of the author(s) only and do not necessarily reflect those of the European Union or the Europe's Rail Joint Undertaking. Neither the European Union nor the granting authority can be held responsible for them. The project Academics4Rails is supported by the Europe's Rail Joint Undertaking and its members.

REFERENCES

[1] White paper on transport – Roadmap to a single European transport area – Towards a competitive and resource efficient transport system [Internet]. 2011. http://europa.eu

[2] Deutsche Bahn 2022 Integrated Report. 2022.

[3] Geischberger J, Moensters M. Impact of faster freight trains on railway capacity and operational quality. *International Journal of Transport Development and Integration*. 2020;4(3):274–85. DOI: 10.2495/TDI-V4-N3-274-285

[4] Quazi A, et al. A field study on the aerodynamics of freight trains with different stacking configurations. *Journal of Wind Engineering and Industrial Aerodynamics.* 2023 Jan 1;232:105245. DOI: 10.1016/j.jweia.2022.105245

[5] Alam F, Watkins S. Lateral stability of a double stacked container wagon under crosswind. *Proceedings of the International Conference on Mechanical Engineering 2007.* 2007.

[6] Li C, et al. Flow topology of a container train wagon subjected to varying local loading configurations. *Journal of Wind Engineering and Industrial Aerodynamics.* 2017;1(169):12–29. DOI: 10.1016/j.jweia.2017.06.011

[7] Flynn D, Hemida H, Baker C. On the effect of crosswinds on the slipstream of a freight train and associated effects. *Journal of Wind Engineering and Industrial Aerodynamics*. 2016;1(156):14–28. DOI: 10.1016/j.jweia.2016.07.001

[8] Sterling M, Baker CJ, Jordan SC, Johnson T. A study of the slipstreams of high-speed passenger trains and freight trains. *Proceedings of the Institution of Mechanical Engineers, Part F: Journal of Rail and Rapid Transit*. 2008;222(2):177–93. DOI: 10.1243/09544097JRRT133

[9] Maleki S, Burton D, Thompson MC. Flow structure between freight train containers with implications for aerodynamic drag. *Journal of Wind Engineering and Industrial Aerodynamics.* 2019:1(188):194–206. DOI: 10.1016/j.jweia.2019.02.007

[10] Flynn D, Hemida H, Soper D, Baker C. Detached-eddy simulation of the slipstream of an operational freight train. *Journal of Wind Engineering and Industrial Aerodynamics*. 2014;132:1–12. DOI: 10.1016/j.jweia.2014.06.016

[11] Bell J, et al. The effect of loading configuration on the slipstream of freight trains. In: *Proceedings of the Sixth International Conference on Railway Technology: Research, Development and Maintenance*. Civil-Comp Press; 2024. p. 1–14.

[12] Alam F, Watkins S. *Effects of crosswinds on double stacked container wagons*. Gold Coast, Australia; 2007 Dec.

[13] Buhr A, Siegel L, Bell J, Henning A. Energy savings for freight trains with aerodynamically optimized loading schemes. *Proceedings of the Sixth International Conference on Railway Technology: Research, Development and Maintenance.* Edinburgh: Civil-Comp Press; 2024. DOI: 10.4203/ccc.7.3.2

[14] Siegel L, Buhr A, Bell J, Henning A. Analysis of flow structures in different loading gaps of freight trains. *Proceedings of the Sixth International Conference on Railway Technology: Research, Development and Maintenance*. Edinburgh: Civil-Comp Press; 2024. DOI: 10.4203/ccc.7.3.1

[15] Giappino S, Rocchi D, Schito P, Tomasini G. Cross wind and rollover risk on lightweight railway vehicles. *Journal of Wind Engineering and Industrial Aerodynamics*. 2016;(1)153:106–12. DOI: 10.1016/j.jweia.2016.03.013

[16] Kocoń A, Flaga A. Critical velocity measurements of freight railway vehicles roll-over in wind tunnel tests as the method to assess their safety at strong cross winds. *Journal of Wind Engineering and Industrial Aerodynamics*. 2021;11:104559. DOI: 10.1016/j.jweia.2021.104559

[17] Soper D, Baker C, Sterling M. Experimental investigation of the slipstream development around a container freight train using a moving model facility. *Journal of Wind Engineering and Industrial Aerodynamics.* 2014;(1)135:105–17. DOI: 10.1016/j.jweia.2014.10.001

[18] Soper D, Baker C. A full-scale experimental investigation of passenger and freight train aerodynamics. *Proceedings of the Institution of Mechanical Engineers, Part F: Journal of Rail and Rapid Transit*. 2020;234(5):482–97. DOI: 10.1177/0954409719844431

[19] Versteeg HK, Malalasekera W. An introduction to computational fluid dynamics - The finite volume method [Internet]. 2007. http://www.pearsoned.co.uk/versteeg

[20] Wang S, et al. The performance of different turbulence models (URANS, SAS and DES) for predicting high-speed train slipstream. Journal of Wind Engineering and Industrial Aerodynamics. 2017;165:46–57. DOI: 10.1016/j.jweia.2017.03.001

[21] Maleki S, Burton D, Thompson MC. Assessment of various turbulence models (ELES, SAS, URANS and RANS) for predicting the aerodynamics of freight train container wagons. *Journal of Wind Engineering and Industrial Aerodynamics*. 2017 Nov 1;170:68–80. DOI: 10.1016/j.jweia.2017.07.008

[22] Heft AI, Indinger T, Adams NA. Introduction of a new realistic generic car model for aerodynamic investigations. *SAE Technical Paper*. 2012. DOI: 10.4271/2012-01-0168

[23] Terra W, et al. A generic cyclist model for aerodynamic investigation: Design, geometry & first aerodynamic analysis of a male time-trial and sprint model. *Journal of Wind Engineering and Industrial Aerodynamics*. 2024 Sep 1;252:105829. DOI: 10.1016/j.jweia.2024.105829

[24] Giannelis NF, Bykerk T, Vio GA. A generic model for benchmark aerodynamic analysis of fifth-generation high-performance aircraft. *Aerospace*. 2023;10(9):746. DOI: 10.3390/aerospace10090746

[25] Bykerk T. A standard model for the investigation of aerodynamic and aerothermal loads on a re-usable launch vehicle. *Aerospace Europe Conference 2023*. 2023.

[26] Principe E. Il Veicolo Ferroviario. Collegio Ingegneri Ferroviari Italiani, editor. Roma: Collegio Ingegneri Ferroviari Italiani; 2010. 29–31 p.

[27] Baker C, et al. *Train aerodynamics: Fundamentals and applications*. Cambridge: Butterworth-Heinemann; 2019.

[28] Corniani L, Schito P, Bruni S. A4R-freight-train-model-geometries. [Accessed 8th Sep 2025]. https://github.com/lCornianiPolimi/A4R-Freight-Train-Model-Geometries

[29] Corniani L, Schito P, Bruni S. Aerodynamics of freight trains: An open database of geometries for CFD analyses. *Proceedings of the sixth international conference on railway technology: Research, development and maintenance.* Edinburgh: Civil-Comp Press; 2024. DOI: 10.4203/ccc.7.3.20

[30] Östh J, Krajnović S. A study of the aerodynamics of a generic container freight wagon using Large-Eddy Simulation. *Journal of Fluids and Structures*. 2014;44:31–51. DOI: 10.1016/j.jfluidstructs.2013.09.017